Journal of ELECTRONIC MATERIALS, Vol. 39, No. 11, 2010
DOI: 10.1007/s11664-010-1351-9
© 2010 TMS

Influence of Palladium Thickness on the Soldering Reactions Between Sn-3Ag-0.5Cu and Au/Pd(P)/Ni(P) Surface Finish

W.H. WU,[1] C.S. LIN,[1] S.H. HUANG,[1] and C.E. HO[1,2]

1.—Department of Chemical Engineering & Materials Science, Yuan Ze University, Chungli City, Taiwan, R.O.C. 2.—e-mail: ceho1975@hotmail.com

This study provides a comparison of the influence of Pd(P) thickness on reactions during soldering with the Sn-3Ag-0.5Cu alloy. Soldering was carried out in an infrared-enhanced conventional reflow oven, and a multiple reflow test method (up to ten cycles) was performed. With increasing Pd(P) thickness, the $(Cu,Ni)_6Sn_5$ grew more slowly at the solder/Ni(P) interface, while the Ni_2SnP/Ni_3P bilayer became predominant after the first reflow. These three intermetallics, i.e., $(Cu,Ni)_6Sn_5$, Ni_2SnP, and Ni_3P, gradually coarsened as the number of reflow cycles increased. Furthermore, an additional $(Ni,Cu)_3Sn_4$ layer appeared between $(Cu,Ni)_6Sn_5$ and Ni_2SnP, especially for the case of a thicker Pd(P) layer (0.2 μm). The attachment of the $(Ni,Cu)_3Sn_4$ to the Ni_2SnP, however, was fairly poor, and a series of microcracks formed along the $(Ni,Cu)_3Sn_4/Ni_2SnP$ interface. To quantify the mechanical response of the interfacial microstructures, shear testing was conducted at two different shear speeds (0.0007 m/s and 2 m/s). The results indicated that the interfacial strength and the Pd(P) thickness were strongly correlated.

Key words: Au/Pd(P)/Ni(P), Pd(P) thickness, Sn-Ag-Cu, interfacial reaction, shear test, Ni_2SnP

INTRODUCTION

Due to environmental concerns regarding lead toxicity, regulations eliminating lead-based materials from electronic products have been imposed in recent decades. Several types of viable surface finishes are suitable for lead-free soldering, such as electrolytic Ni/Au, electroless Ni/immersion Au (ENIG), immersion tin, immersion silver, and organic solderability preservative. Among finishing techniques, ENIG is often used in high-end microelectronic packages. The Au layer of ENIG provides good oxidation resistance and excellent wettability for Sn-based solders.[1–3] Although the thickness of the immersion Au layer is only one-tenth of the electrolytic-type Au, it can be used to bond gold wires as well.[4] Electroless Ni contains approximately 7 wt.% to 10 wt.% P in the Ni matrix and has an amorphous structure that can serve as a diffusion barrier, preventing the rapid reactions between solders and Cu.[2,3,5] However, galvanic hypercorrosion in the Ni(P) layer caused by immersion gold solution can result in the formation of Ni oxides over in the Ni(P) surface, which reduces the reliability of the joint interface.[6–10] This reliability concern is usually termed "black pad" and becomes more serious in miniaturized packages, necessitating a significant increase in the solder joint number and a decrease in joint size.

To improve the reliability of ENIG, an additional Pd (or Pd-P) layer has been introduced in the Au/Ni(P) bilayer to prevent the direct attack of Ni(P) by the gold plating bath. The key difference between the Pd deposition mechanism and immersion Au plating is that the former is deposited by chemical reduction instead of displacement reaction as in the latter process. As a result, significantly less corrosion is observed in the Ni(P) layer during the Pd plating process. Other advantages of the Pd layer include lower production cost and higher compatibility with wire-bonding processes.[11] A Pd layer can

(Received March 31, 2010; accepted August 2, 2010; published online September 4, 2010)

be successfully applied to wire bonds because the Pd can act as an effective diffusion barrier, preventing underlying Ni from diffusing to the Au surface as Ni oxides.[12] Moreover, Pd has a higher hardness than Au (Pd: 250 HV to 300 HV; Au: 60 HV to 100 HV), providing better mechanical support.[13]

The objective of the present study is to evaluate the soldering reactions between a Au/Pd(P)/Ni(P) trilayer (i.e., ENEPIG) and a Sn-3Ag-0.5Cu alloy (i.e., 96.5Sn-3Ag-0.5Cu, wt.%). In soldering applications, the thickness of the Pd layer can vary from 0.05 μm to 0.3 μm. However, data for the effect of Pd thickness on solderability are still seriously lacking, especially for joining with the Sn-Ag-Cu family of alloys.[14,15] In this study, the thickness of the Pd(P) layer was varied (0 μm, 0.1 μm, and 0.2 μm), and the interfacial reactions that occurred during soldering were investigated. The morphology of the intermetallic species that formed from various Pd(P) layers under different soldering conditions were examined using scanning electron microscopy (SEM), focused ion beam (FIB), and field-emission transmission electron microscopy (FE-TEM). Furthermore, the mechanical properties of the joints were examined by conducting shear testing at two different shear speeds (0.0007 m/s and 2 m/s).

EXPERIMENTAL PROCEDURES

Figure 1 illustrates the configuration of the joint and thicknesses of the Au/Pd(P)/Ni(P)/Cu metallization pad utilized in this study. The surface finish, Au/Pd(P)/Ni(P), was deposited on Cu pads with a 375-μm opening in a ball grid array (BGA) substrate. The thicknesses of the Au and Ni(P) layers were set to 0.1 μm and 7 μm, and the thickness of the Pd(P) layer was varied from 0 μm (i.e., ENIG) to 0.2 μm. A small amount of P (2% to 5%)/(6% to 8%) was codeposited with the Pd/Ni bilayer due to the use of an alkaline solution of hypophosphite, as evidenced by micro electron spectroscopy for chemical analysis (μ-ESCA) and electron probe microanalysis (EPMA).[16] The solder balls used in this study consisted of 96.5 wt.%Sn-3 wt.%Ag-0.5 wt.%Cu (termed Sn-3Ag-0.5Cu) and had a diameter of 500 μm. Before soldering, the solder balls were dipped into rosin mildly activated (RMA) flux and planted on the Au/Pd(P)/Ni(P) pads (Fig. 1). During soldering, the substrates were subjected to heating in an infrared-enhanced conventional reflow oven. The peak reflow temperature was set to 260°C, and the reflow time was 80 s. A multiple reflow process with one, five, or ten cycles was performed.

After reflow(s), the interior microstructures of the joints were revealed through a metallographical grinding/polishing process. The polished specimens were subjected to FIB to reduce mechanical-polishing-induced artificial damage and to elucidate the contrast between $(Cu,Ni)_6Sn_5$ and $(Ni,Cu)_3Sn_4$.[17] The composition of each phase was determined using EPMA operated at 15 keV. During the

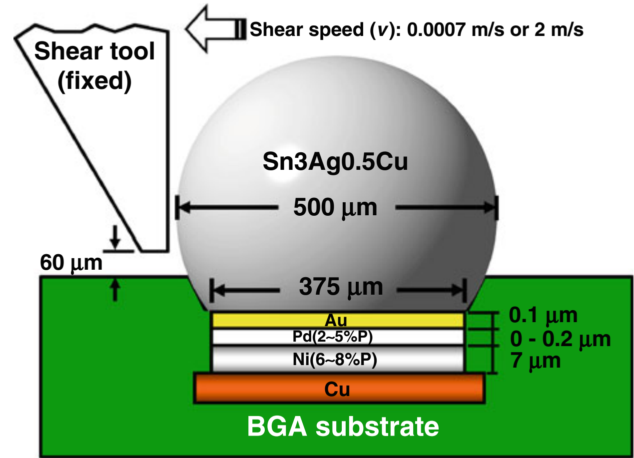

Fig. 1. Schematic diagram of a Sn-3Ag-0.5Cu/Au/Pd(P)/Ni(P)/Cu solder joint in a shear test. Shear speeds (v) of 0.0007 m/s and 2 m/s were applied.

measurement, Au L_α, Pd L_α, Ni K_α, P K_α, Sn L_α, and Cu K_α x-rays were detected. The concentration of each element was measured independently, and the total weight percentage was 100 ± 1%. For each data point, at least three measurements were made, and the average value is reported. Moreover, FE-EPMA (operated at 12 keV) and FE-TEM (operated at 80 keV) were utilized to identify phase domains with a diameter of less than 1 μm.

To evaluate the effect of Pd(P) thickness on the mechanical properties of the joints, a batch of solder joints was subsequently examined through a ball shear test. The shear test was carried out using DAGE bond testers (types 4000 and 4000HS), according to the JESD22-B117 standard.[18] Shear speeds of 0.0007 m/s and 2 m/s were employed, and the shear height was fixed at 60 μm (Fig. 1). For each data point, at least 15 measurements were made, and the average was reported. After shearing, SEM energy-dispersive x-ray (EDX) analysis and μ-ESCA were utilized to identify the fracture surface. In the depth analysis, a sputtering rate of 18.75 nm/min was applied, according to a known SiO_2 film etched using a Ga^+ beam.

RESULTS

Soldering Reactions Between Sn-3Ag-0.5Cu and Au/Pd(P)/Ni(P)

Figure 2 shows the interfacial microstructures between Sn-3Ag-0.5Cu and Au/Pd(P)/Ni(P) after the first (Fig. 2a–d) and tenth reflow (Fig. 2e–h). The thickness of the Au layer prior to soldering was 0.1 μm, and the thickness of the Pd(P) layer was 0 μm (Fig. 2a, e), 0.1 μm (Fig. 2b, f), and 0.2 μm (Fig. 2c, d, g, h). As shown in Fig. 2a, two intermetallic layers, i.e., $(Cu,Ni)_6Sn_5$ (upper region) and Ni_3P (lower region), were formed at the solder/Ni(P) interface after the first reflow. The formation of

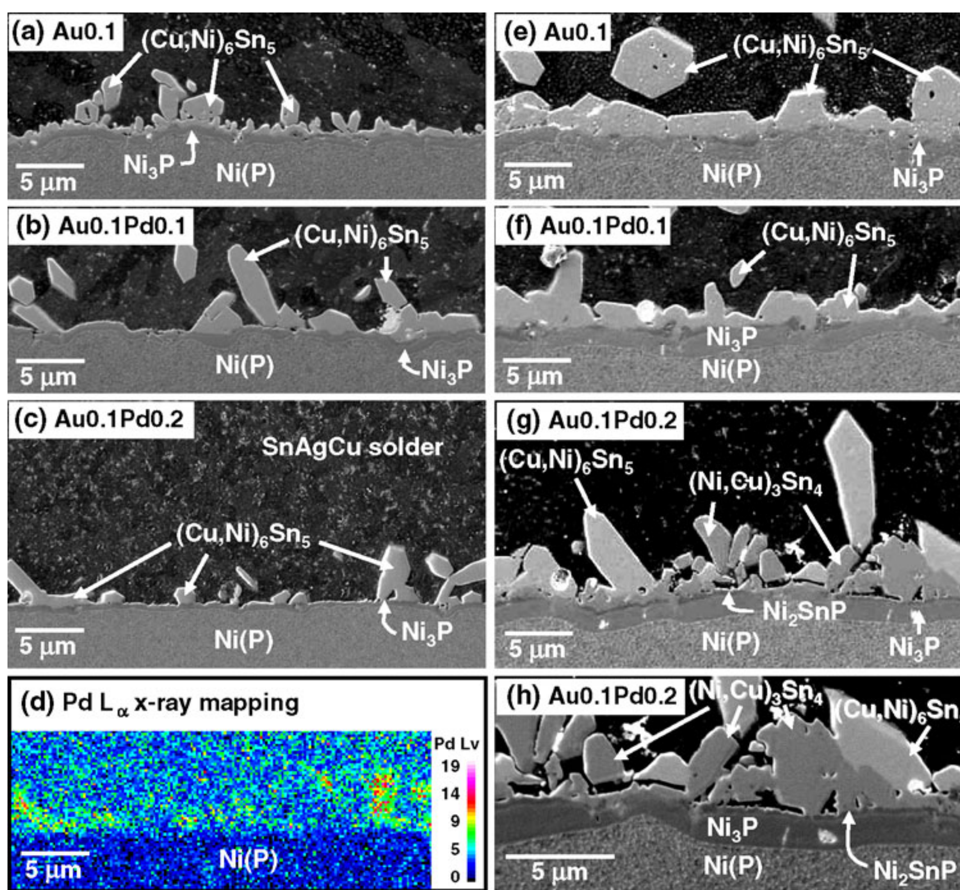

Fig. 2. FIB micrographs showing the reaction zones between Sn-3Ag-0.5Cu and Au/Pd(P)/Ni(P) after the first (a–c) and tenth reflow (e–g). The thickness of the Au layer was 0.1 μm, and the thickness of the Pd(P) layer was 0 μm (a, e), 0.1 μm (b, f), and 0.2 μm (c, g). (d) EPMA Pd L_α x-ray mapping of the reaction zone shown in (c); (h) magnification of the solder/Ni(P) interface in (g).

$(Cu,Ni)_6Sn_5$ at the solder/Ni interface is consistent with the results of previous studies,[3,19–21] where the concentration of Cu in solders was greater than or equal to 0.5 wt.%. A possible mechanism for the formation of $(Cu,Ni)_6Sn_5$ is provided in the literature.[3,19–21] The morphology of the reaction products changed with the use of the Pd(P) layer, as can be noted in Fig. 2b and c. When 0.1-μm-thick Pd(P) was deposited for soldering, the $(Cu,Ni)_6Sn_5$ layer became discontinuous and the Ni_3P thickness decreased (Fig. 2a, b). The evolution in the microstructure was readily apparent when the Pd(P) thickness was further increased to 0.2 μm (Fig. 2c). Moreover, the introduction of an additional Pd(P) layer altered the composition of $(Cu,Ni)_6Sn_5$. Figure 2d shows the distribution of Pd x-rays throughout the reaction zone shown in Fig. 2c. The results indicated that a small amount of Pd was incorporated into the $(Cu,Ni)_6Sn_5$ grains after soldering.

To demonstrate the effect of Pd(P) on the $(Cu,Ni)_6Sn_5$ morphology, solder caps of similar joints were etched with nitric acid solution at room temperature. As shown in Fig. 3, a bird's-eye view of the interfaces clearly reveals the difference in the $(Cu,Ni)_6Sn_5$ grains. The $(Cu,Ni)_6Sn_5$ produced via ENIG (Fig. 3a) exhibited a pike-like, dense morphology, while that produced via electroless nickel/electroless palladium (ENEP) (Fig. 3b and c) was hexagonal and rod like. Moreover, in regions without covering with $(Cu,Ni)_6Sn_5$, the Ni(P) nodules were exposed accordingly. The finding above suggests that the Pd(P) layer had a significant effect on the interfacial reaction, although it would convert into $(Pd,Ni)Sn_4$ grains first and sequentially spalled away from the reaction zone at the early stage of soldering.[16]

It is also worth noting that many submicrometer facet-type grains grew on the surface of the Ni(P) nodules (Fig. 3b). These grains may be derived from $(Cu,Ni)_6Sn_5$ crystals that nucleated on the substrate or the other phase(s) that enabled coexistence with $(Cu,Ni)_6Sn_5$. To identify the observed phases, a thin-film specimen prepared via FIB was examined by FE-TEM at 80 keV. Figure 4 shows TEM-EDX elemental mappings of the reaction zone shown in Fig. 2c. In regions without growing $(Cu,Ni)_6Sn_5$, a compound layer between the solder and Ni_3P was observed. Moreover, EDX mapping (Fig. 4b–g) results indicated that the compound consisted primarily of Ni, Sn, and P, and significant amounts of Au, Pd, and Cu were not observed. Thus, the grains

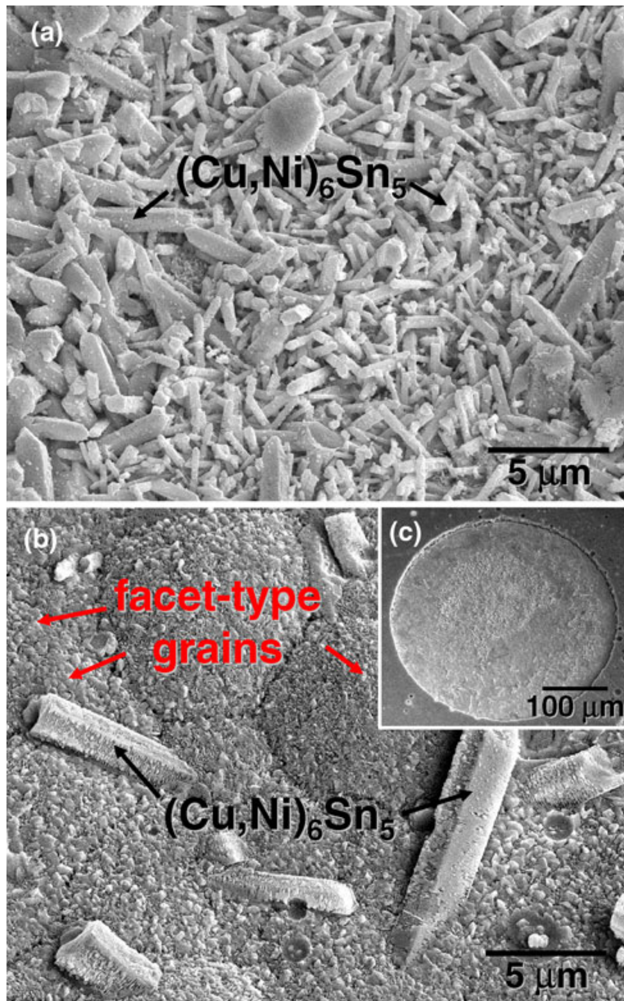

Fig. 3. Top-view micrographs showing the morphology of the reaction product(s) produced via ENIG [Au(0.1 μm)/Pd(P)(0 μm)/Ni(P)] (a) and ENEP [Au(0 μm)/Pd(P)(0.1 μm)/Ni(P)] (b). (c) Full view of the micrograph shown in (b).

that grew on the Ni(P) nodules (Fig. 3b) were a Ni-Sn-P ternary compound. Below the Ni-Sn-P layer, a portion of Pd remained at the interface, as shown in Fig. 4f. A possible mechanism for the formation of a Ni-Sn-P ternary compound will be presented in the "Discussion" section.

Figure 5a displays a TEM bright-field micrograph of the solder/Ni(P) interface shown in Fig. 4a. As shown in the figure, the Ni-Sn-P layer was approximately 0.3 μm thick. With the aid of the TEM-EDX quantitative analysis (Fig. 5b–d), the phases above and below the Ni-Sn-P layer (labeled "b" and "d" in Fig. 5a) were the Sn-rich and Ni_3P phase, respectively. In contrast, the average composition of the Ni-Sn-P layer (labeled "c") was 56.5 at.% Ni, 25.4 at.% Sn, and 18.1 at.% P, which is similar to the composition of the Ni_2SnP phase reported in the literature[22–26] (Table I). The crystal structure of Ni_2SnP was orthorhombic (lattice constant: a = 1.28260 nm, b = 0.35943 nm, c = 0.50896 nm; space group: $Pnma$)[27] and was further verified through TEM electron diffraction analysis.[23,24,28] Therefore, the results indicated that the small Ni-Sn-P grains on the Ni(P) surface (Fig. 3b) were likely Ni_2SnP. Between Ni_2SnP and Ni_3P, there were several possible intermediate phases, e.g., Ni_2P and $Ni_{12}P_5$, which were also resolved in the Sn-3Ag-0.5Cu/Ni(P) case by Duh and colleagues.[22–24] However, Ni_2P and $Ni_{12}P_5$ were more stable under the condition that the P content in the Ni(P) metallization was high ($\sim$13 wt.%),[22–24] instead of the $\sim$7 wt.% P content utilized in this study. Therefore, Ni_2P and $Ni_{12}P_5$ may not be present in the reaction zone due to thermodynamic constraints. Another possibility is that these missing phases were too thin to be resolved. To verify this hypothesis, more careful examination of the interface via high-resolution TEM must be conducted.

According to the results of Duh and colleagues,[22–24] the Ni_2P plays a key role in the growth of Ni_2SnP that nucleated through Sn diffusion into the Ni_2P. When the P content of the Ni metallization was low (e.g., Ni-7 wt.%P), only minor amounts of Ni_2SnP were formed due to the lack of Ni_2P.[22,24] However, in the present study, significant growth was observed at a P content of about 7 wt.%, as depicted in Figs. 2, 4, and 5. The dependence of Ni_2SnP growth on the thickness of the Pd(P) layer will be discussed in subsequent sections. In short, the $(Cu,Ni)_6Sn_5$ decreased, and the Ni_2SnP and Ni_3P became the dominant phases at the interface when a thick Pd(P) layer was deposited between Au and Ni(P) for soldering.

The morphology of intermetallic species was dependent on the number of reflows. As shown in Fig. 2e–h, the intermetallic(s) layer obtained after the tenth reflow was coarser than that of the first reflow. The morphology of the $(Cu,Ni)_6Sn_5$ became layered type for all cases. Additionally, the Ni_3P and Ni_2SnP increased with increasing Pd(P) thickness. In the case of using thick Pd(P) (Fig. 2g, h), the resulting Ni_2SnP grew to a thickness of over 0.5 μm, which allowed us to measure its composition accurately by FE-EPMA; the atomic ratio of Ni_2SnP was 51.0:27.2:21.8, which is consistent with the results listed in Table I. The $(Ni,Cu)_3Sn_4$ was also observed, specifically in regions without $(Cu,Ni)_6Sn_5$ (Fig. 2g, h). Interestingly, most of the $(Ni,Cu)_3Sn_4$ was not well adhered to the Ni_2SnP phase, and resulted in cracking in the interface. Spalling of $(Ni,Cu)_3Sn_4$ from the interface was strongly correlated to the formation of Ni-Sn-P, as reported previously in the literature.[22,24,26,29–31] Mechanical response of the microcracks was provided in the following section.

Shear Test Results

To quantify the mechanical response of the interfacial microstructures, shear testing at two different shear speeds, 0.0007 m/s and 2 m/s, was

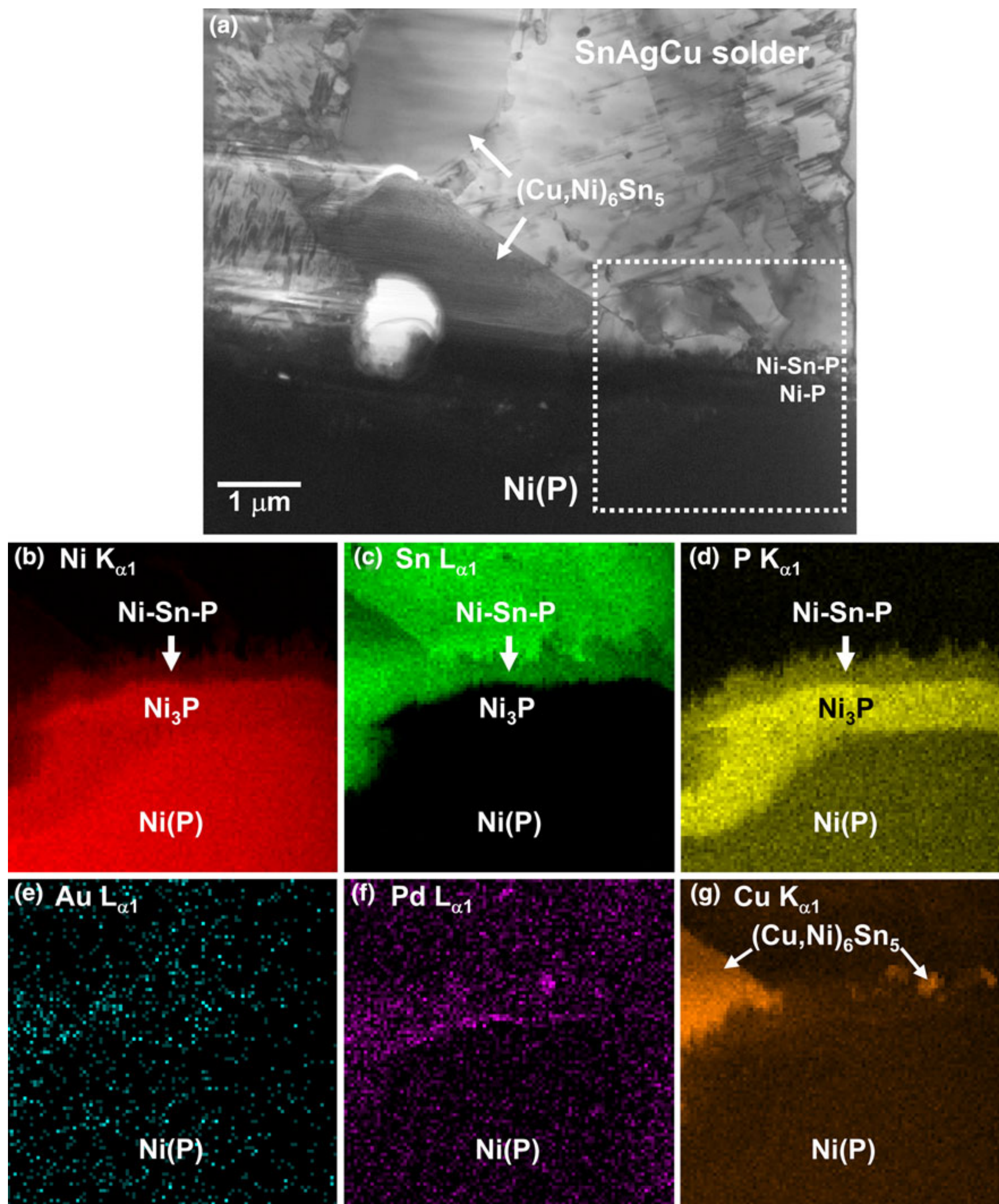

Fig. 4. (a) TEM bright-field image of a reaction zone similar to the one shown in Fig. 2c; (b–g) TEM EDX elemental mappings of the dotted area in (a) for: Ni (b), Sn (c), P (d), Au (e), Pd (f), and Cu (g).

conducted. Figure 6a shows typical shear strength–displacement curves obtained under the aforementioned experimental conditions. The abrupt curve produced by the high-speed test (the dotted curve) indicated that the joint suffered serious damage before the shear tool (Fig. 1) passed through the entire pad. This failure mode is a typical brittle type, and the resulting fracture usually occurs along the solder/pad interface due to the presence of brittle intermetallic compounds (IMCs), as shown in Fig. 6b. In contrast, the curve displayed in the low-speed test was considerably smoother, indicating a ductile failure mode. As shown in Fig. 6c, the ductile failure occurred above the surface of the solder mask within the bulk solder region where an obvious shear band along the shear direction was created. Figure 6d shows the interfacial shear strength as a function of the number of reflow cycles and the thickness of the Pd(P) layer. The results of the low-speed shear test (broken lines in Fig. 6d) did not

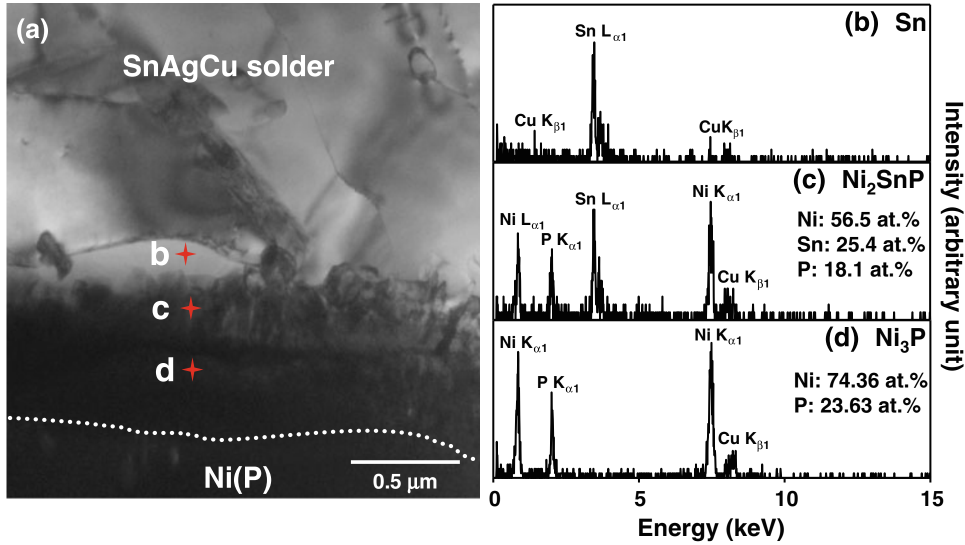

Fig. 5. (a) TEM bright-field image showing a zoomed-in view of the solder/Ni(P) interface of Fig. 4a; (b–d) TEM-EDX spectra for the corresponding labeled points in (a).

Table I. Quantitative analysis of the Ni_2SnP through TEM-EDX, FE-EPMA, and EPMA

Composition of Ni_2SnP				
Apparatus	**Ni (at.%)**	**Sn (at.%)**	**P (at.%)**	**Reference**
TEM-EDX	56.5	25.4	18.1	This study
	53.5	26.3	20.3	Refs. 23 and 24
	45.9	28.4	25.9	Ref. 25
FE-EPMA	51.0	27.2	21.8	This study
	49.8 ± 0.2	28.1 ± 0.2	22.2 ± 0.2	Refs. 22–24
EPMA	40.5–47.8	25.6–31.8	26.6–28.1	Ref. 26

reflect a significant difference among various numbers of reflow cycles and Pd(P) thickness, because the failure occurred primarily in the solder region that did not change enormously in comparison with the interfacial microstructures.

Compared with the results of the low-speed test, the shear strength obtained from the high-speed test (solid lines in Fig. 6d) was rather sensitive to the number of reflow cycles. The interfacial strength decreased dramatically with increasing number of reflow cycles, regardless of the thickness of the Pd(P) layer. In the high-speed test, significant fractures were observed along the solder/Ni(P) interface, as demonstrated in Fig. 6b. When the Pd(P) layer was approximately 0.1 μm thick, the interfacial strength of the joint was approximately 200 g greater than the strength of a joint without a Pd layer (ENIG), suggesting that a small amount of Pd(P) would enhance the interfacial strength of the joint. Moreover, after the first reflow, the interfacial strength increased with increasing thickness of the Pd(P) layer, as shown in Fig. 6d. The highest strength was observed when a 0.2-μm-thick Pd(P) layer was employed, and the lowest strength was observed when the Pd layer was completely omitted. These results suggest that the formation of the solder/Ni_2SnP/Ni_3P interfaces was more beneficial to the mechanical properties of the joints than the formation of solder/$(Cu,Ni)_6Sn_5$/Ni_3P interfaces (Fig. 2a–c). Interestingly, in the case of 0.2 μm Pd(P), the strength dramatically decreased with increasing number of reflow cycles (Fig. 6d). After the tenth reflow cycle, the strength of the joints decreased by approximately 35% and displayed the lowest strength. The fact that significant cracks existed along the $(Ni,Cu)_3Sn_4$/Ni_2SnP interface before the test (Fig. 2g, h) may be the root cause for the dramatic decrease in strength. In short, deposition of an adequate Pd(P) layer between Au and Ni(P) was beneficial to the mechanical properties of the joints. However, the reliability of the joints was degraded significantly after multiple reflow cycles when the Pd(P) layer was thick ($\sim$0.2 μm).

Figure 7 shows the fraction of the joints that failed along the interface after the high-speed shear test. Failure was defined as interfacial if greater than 90% of the fracture surface was located along

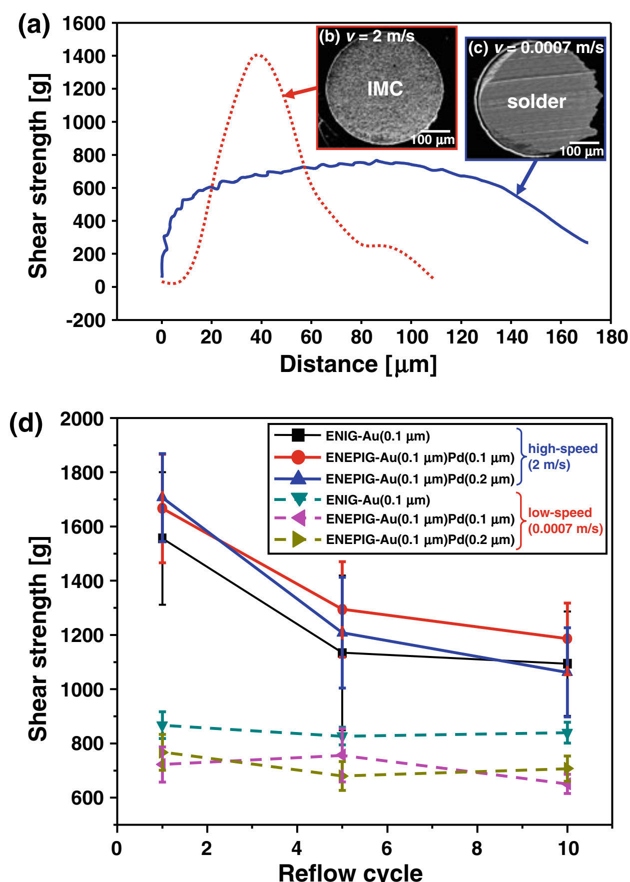

Fig. 6. (a) Shear strength–displacement curves of the high- (v = 2 m/s) and low-speed (v = 0.0007 m/s) shear tests. (b, c) Top-view micrographs of the fracture surfaces of brittle (b) and ductile (c) failure modes. (d) The shear strength of the joints as a function of the Pd(P) layer thickness and the reflow cycle. Solid and broken lines correspond to the results of high- and low-speed shear tests, respectively.

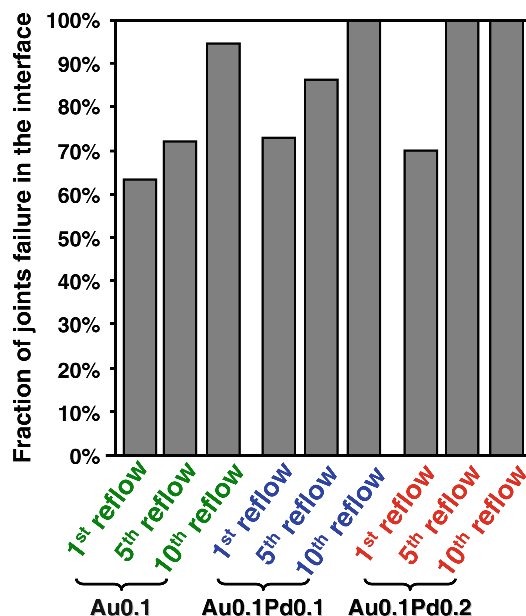

Fig. 7. The fraction of Sn-3Ag-0.5Cu/Au/Pd(P)/Ni(P) joints that failed at the interface after the high-speed shear test.

the solder/Ni(P) interface. The results indicated that more than 60% of the joints failed due to interfacial fracture during high-speed impact. Interestingly, this fraction increased with increasing number of reflow cycles or thickness of the Pd(P) layer. The increase in the number of brittle intermetallic species (Fig. 2e–g) and the presence of the microcracks along the $(Ni,Cu)_3Sn_4/Ni_2SnP$ interface (Fig. 2g, h) were likely the underlying mechanisms for the observed trend.

Figure 8a shows a side-view picture of the interfacial fracture of a Sn-3Ag-0.5Cu/Au(0.1 μm)/Pd(P)(0.2 μm)/Ni(P)/Cu joint. Cracking in the joint occurred along the $(Cu,Ni)_6Sn_5$/Ni(P) interface, as can be observed in this figure. To investigate joint failure in more detail, a similar fracture surface was examined by μ-ESCA. Figure 8b shows depth profiles of the atomic concentrations on the surface, as indicated by a red circle in Fig. 8c. As shown in Fig. 8b, the surface region (0 nm to 30 nm in depth) primarily consisted of Sn, Ni, and Cu (ranked by concentration), suggesting that the fracture occurred near $(Ni,Cu)_3Sn_4$. Below 400 nm, the concentration of P and Ni increased to a 1:3 ratio, indicating the presence of Ni_3P. Between 30 nm and 400 nm, the concentration of Ni and P increased, and that of Sn and Cu decreased. The composition of the region was 35 at.% to 65 at.% Ni, 15 at.% to 35 at.% Sn, 9 at.% to 19 at.% P, and a balance of Cu, suggesting that the region consisted primarily of a Ni-Sn-P compound, and little overlap from the upper [i.e., $(Ni,Cu)_3Sn_4$] and lower region (i.e., Ni_3P) was observed. The combined results indicated that the Ni-Sn-P compound was Ni_2SnP. In other words, fracture occurred around the $(Ni,Cu)_3Sn_4/Ni_2SnP$ interface.

DISCUSSION

The most interesting finding in this study is the difference of the interfacial microstructures between ENIG and ENEPIG soldering systems (Figs. 2 and 3). A dense, continuous layer of $(Cu,Ni)_6Sn_5$ was observed in the ENIG case after the first reflow (Figs. 2a and 3a); nevertheless, in the ENEPIG case, the Ni_2SnP exhibited a continuous layer with a small amount of $(Cu,Ni)_6Sn_5$ grains scattered near the interface (Figs. 2b, c and 3b). These features were readily apparent when a thick Pd(P) layer was employed. The possible mechanism associated with the Ni_2SnP growth in the ENEPIG case is discussed below.

Figure 9 displays a schematic depiction of the atomic fluxes of Pd, Ni, Sn, and P of the soldering reaction between a Sn-Ag-Cu alloy and a Au/Pd(P)/Ni(P) trilayer. The Au is not illustrated in the figure because it would react quickly to form $AuSn_4$

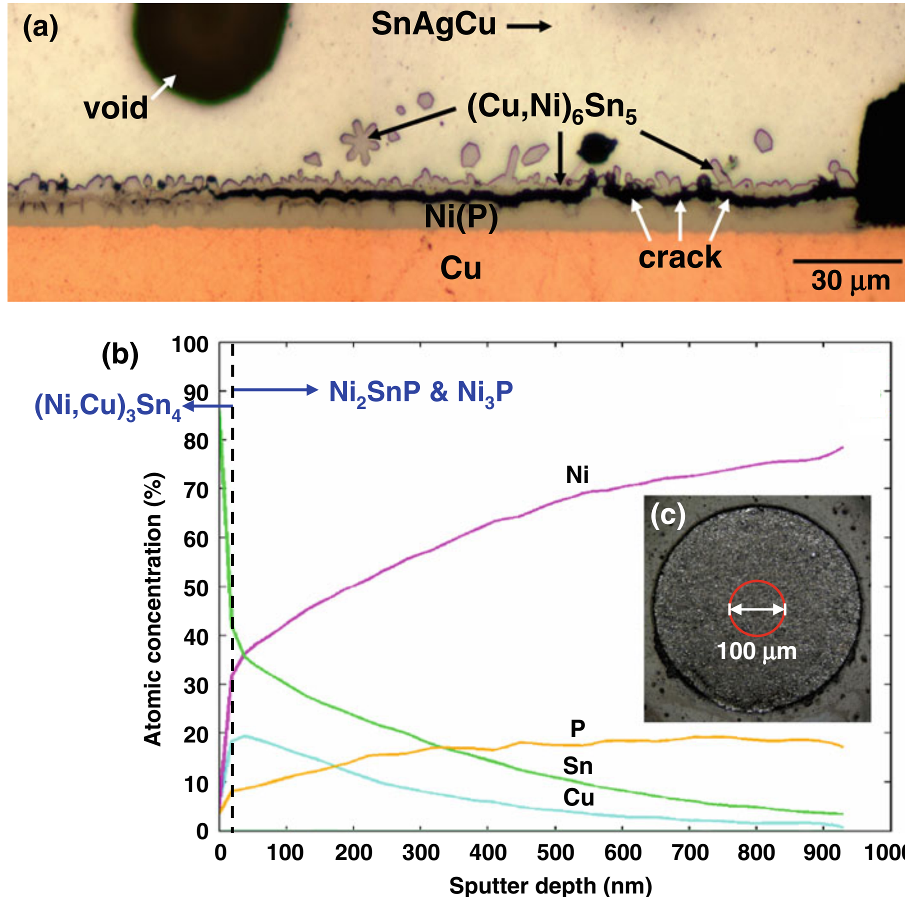

Fig. 8. (a) Optical micrograph of an interfacial fracture of a Sn-3Ag-0.5Cu/Au(0.1 μm)/Pd(P)(0.2 μm)/Ni(P)/Cu joint that was reflowed ten times and subjected to a manual shear test. (b) μ-ESCA depth profiles of the atomic concentrations of the fracture surface as a function of the sputter depth. (c) Top-view micrograph of the fracture surface of a joint that is similar to the one shown in (a) after a high-speed shear test. The μ-ESCA analysis was performed on the region highlighted in (c) by a red circle.

[or $(Au,Ni)Sn_4$] and spall into the molten solder within seconds.[32] Additionally, the Au in solder did not significantly affect the reaction of the Pd(P)/Ni(P).[16] After the Au disappeared from the interface, the underlying metallization layer, i.e., the Pd(P) layer, was exposed. The soldering reaction of Pd is just as complicated as that of Au,[14,15] but only $PdSn_4$ is depicted in Fig. 9 for brevity. The depletion process of Pd in the molten solder is similar to that of Au in two ways. First, the Pd would be quickly converted into $PdSn_4$ [or $(Pd,Ni)Sn_4$],[14–16] which has a similar crystal structure to $AuSn_4$.[33] Additionally, this compound would break from the root of grains and then separate from the interface during soldering.[14,16] These two tightly connected processes can be achieved within a few seconds according to the evidence provided in the cited literature,[16] where a trilayer of Au(0.1 μm)/Pd(P)(0.2 μm)/Ni(P) wetted with Sn-3Ag-0.5Cu at 240°C was investigated. In the present study, the Pd layer was not as pure as the Au layer but instead incorporated 2 wt.% to 5 wt.% P owing to the plating process. After the Pd was fully consumed, the P that existed within the Pd(P) layer separated from the interface, as depicted in Fig. 9. Subsequently, the P crystallized with Sn and Ni at the interface to form Ni_2SnP. More Ni_2SnP accumulated at the interface is anticipated when a thicker Pd(P) layer is employed for soldering. Thus, the P in the Ni_2SnP was derived primarily from the Pd(P) layer, instead of the underlying Ni(P) layer. This hypothesis was corroborated by the dependence of the Ni_2SnP quantity on the thickness of the Pd(P) layer (Fig. 2a–c). The aforementioned reaction mechanism also provides a possible explanation for why a significant Ni_2SnP layer could be created in the Ni-7 wt.%P case.

The resettlement of the P to the interface is not unique to the soldering reaction, and a similar reaction mechanism had also been proposed by Tu and colleagues.[5] In that study,[5] the Ni within the Ni(P) layer was depleted by the soldering reaction, and the P crystallized with Ni(P), resulting in the growth of Ni_3P at the interface. However, unlike the formation of Ni_3P,[5] the growth of Ni_2SnP in the present study resulted from depletion of the Pd(P) layer. As a result, the growth of the latter was significantly faster than the former, because the soldering reaction of Pd/solder was orders of

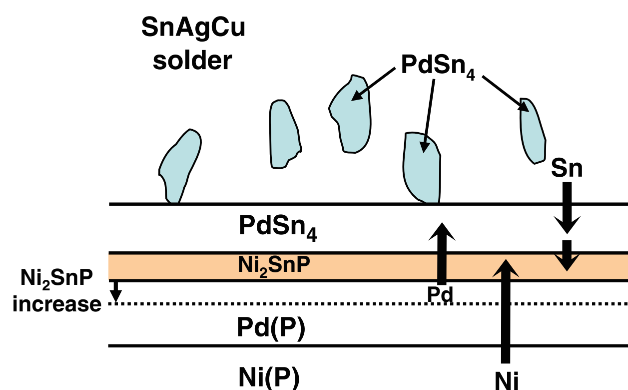

Fig. 9. Schematic diagram illustrating the growth of Ni_2SnP and the atomic fluxes of Pd, Ni, Sn, and P during a soldering reaction of a Sn-Ag-Cu solder with a Au/Pd(P)/Ni(P) trilayer. In this study, the P content in the Pd and Ni layer were 2 wt.% to 5 wt.% and 6 wt.% to 8 wt.%, respectively. The Au and Ni_3P layers are not drawn for brevity.

magnitude faster than that of Ni/solder,[34,35] despite the fact that the P content (2% to 5%) of the Pd(P) layer was lower than that of the Ni(P) layer. The rapid growth of a dense Ni_2SnP layer at the interface may prevent the solder from reaching the underlying Pd(P) layer, causing a portion of the Pd to become buried beneath Ni_2SnP, as demonstrated in Fig. 4f. Further studies must be conducted to determine whether the Pd can be removed completely by long-term soldering reactions.

Another interesting observation that must be explained is that the growth of $(Cu,Ni)_6Sn_5$ produced via ENEPIG was discontinuous (Figs. 2b, c and 3b). One hypothesis is that the interfacial energy had a significant effect on the growth of $(Cu,Ni)_6Sn_5$. If the interfacial energy of $(Cu,Ni)_6Sn_5$/Ni_2SnP was larger than that of solder/Ni_2SnP, the formation of the solder/Ni_2SnP interface became more stable than growing a layered-type $(Cu,Ni)_6Sn_5$ onto the Ni_2SnP. In other words, the Ni_2SnP preferred to be in direct contact with the solder than $(Cu,Ni)_6Sn_5$. As a result, the growth of $(Cu,Ni)_6Sn_5$ was limited once the interface was covered with a layer of Ni_2SnP. However, the results of long-term soldering reactions (Fig. 2e–g) suggested that this hypothesis was incorrect, and a layer of $(Cu,Ni)_6Sn_5$ could be created if multiple reflows were conducted (Fig. 2f, g). This implies that interfacial energy is not a key factor for the different $(Cu,Ni)_6Sn_5$ morphology. In ENEPIG, a $(Cu,Ni)_6Sn_5$ layer did not immediately develop after the first reflow (Figs. 2b, c and 3b), and the Ni_2SnP layer expanded as P became separated from the Pd(P) layer during the early stage of the soldering reaction. In other words, the growth of Ni_2SnP and $(Cu,Ni)_6Sn_5$ were in direct competition, and the growth of the former dominated over the latter during the soldering reaction of Sn-Ag-Cu/Pd(P)/Ni(P). This explains why the morphology of $(Cu,Ni)_6Sn_5$ was dependent on the thickness of the Pd(P) layer, as shown in Fig. 2a–c. Soldering reactions between Sn-Ag-Cu and Ni with an even thicker Pd(P) layer should be conducted to verify this hypothesis.

CONCLUSIONS

The influence of Pd (or Pd-P) thickness on the soldering reactions between Sn-3Ag-0.5Cu and Au/Pd(P)/Ni(P) surface finish was investigated systematically by electron microscopies, and shear tests were conducted to determine the strength of the joints. The major intermetallic species that grew between Sn-3Ag-0.5Cu and Au/Pd(P)/Ni(P) after reflow soldering were $(Cu,Ni)_6Sn_5$, $(Ni,Cu)_3Sn_4$, Ni_2SnP, and Ni_3P. With increasing Pd(P) thickness from 0 μm (i.e., ENIG) to 0.2 μm, the morphology of $(Cu,Ni)_6Sn_5$ became discontinuous, and a Ni_2SnP/Ni_3P bilayer grew at the solder/Ni(P) interface after the first reflow. The dependency of the microstructures on the thickness of the Pd(P) was attributed to the separation of P from the Pd(P) layer during the early stage of the soldering reaction, which nucleated as a dense Ni_2SnP layer that dominated over the growth of $(Cu,Ni)_6Sn_5$. The $(Cu,Ni)_6Sn_5$, Ni_2SnP, and Ni_3P gradually coarsened, and the former became a layered structure over the Ni_2SnP after multiple reflows. The $(Ni,Cu)_3Sn_4$ was observed between the $(Cu,Ni)_6Sn_5$ and Ni_2SnP layers, and significant amounts of $(Ni,Cu)_3Sn_4$ were obtained when a thick (0.2 μm) Pd(P) layer was employed.

Shear tests with speeds of 0.0007 m/s and 2 m/s were utilized to quantify the mechanical response of the interfacial microstructures. The results of the low-speed (0.0007 m/s) test did not reflect changes in the interfacial microstructure but that of the high-speed (2 m/s) test due to the presence of different failure modes. In the low-speed test, the joints typically failed in the solder region. In contrast, in the high-speed tests, failure along the solder/pad interface became predominant. The highest shear strength was obtained after the first reflow cycle when a Pd(P) finish was used; however, after multiple reflows, the strength was dramatically reduced. This is especially valid when a 0.2 μm Pd(P) was deposited for soldering. In this case, i.e., 0.2 μm Pd(P), the fracture occurred along the $(Ni,Cu)_3Sn_4$/Ni_2SnP interface, and a series of microcracks was observed between these two phases. The results of the aforementioned analyses indicated that an adequate Pd(P) thickness (0.1 μm) improves the mechanical properties of these solder joints.

ACKNOWLEDGEMENTS

This study was supported by the National Science Council (R.O.C.) through Grant No. NSC97-2628-E-155-001-MY2 and by Kinsus Interconnect Technology Corp. through Grant No. NSC98-2622-E-155-004-CC3. The authors would also like to acknowledge

Chi-Ming Lin, Dennis Lin (Kinsus Interconnect Technology Corp.), Linda Huang (Schmidt Scientific Taiwan Ltd.), Robert Peng (Taiwan Uyemura Corp. Ltd.), Chung-Yuan Kao (National Taiwan University), and S.Y. Tsai (National Tsing Hua University) for assistance in experimental work.

REFERENCES

1. J. Glazer, *Int. Mater. Rev.* 40, 65 (1995).
2. K.N. Tu and K. Zeng, *Mater. Sci. Eng.* R34, 1 (2001).
3. T. Laurila, V. Vuorinen, and J.K. Kivilahti, *Mater. Sci. Eng.* R49, 1 (2005).
4. A.J.G. Strandjord, S. Popelar, and C. Jauernig, *Microelectron. Reliab.* 42, 265 (2002).
5. J.W. Jang, P.G. Kim, K.N. Tu, D.R. Frear, and P. Thompson, *J. Appl. Phys.* 85, 8456 (1999).
6. P. Snugovsky, P. Arrowsmith, and M. Romansky, *J. Electron. Mater.* 30, 1262 (2001).
7. R.J. Coyle, D.E.H. Popps, A. Mawer, D.P. Cullen, G.M. Wenger, and P.P. Solan, *IEEE Trans. Comp. Packag. Technol.* 26, 724 (2003).
8. K. Zeng, R. Stierman, D. Abbott, and M. Murtuza, *JOM* 58, 75 (2006).
9. K. Suganuma and K.S. Kim, *JOM* 60, 61 (2008).
10. B.K. Kim, S.J. Lee, J.Y. Kim, K.Y. Ji, Y.J. Yoon, M.Y. Kim, S.H. Park, and J.S. Yoo, *J. Electron. Mater.* 37, 527 (2008).
11. P. Ratchev, S. Stoukatch, and B. Swinnen, *Microelectron. Reliab.* 46, 1315 (2006).
12. W. Sun, W.H. Zhu, E.S.W. Poh, H.B. Tan, and R.T. Gan, *Proceeding of International Conference on Electronic Packaging Technology & High Density Packaging, ICEPT-HDP* (2008), p. 1.
13. Y. Oda, M. Kiso, S. Kurosaka, A. Okada, K. Kitajima, and S. Hashimoto, *Proceeding of International Microelectronics & Packaging Society, IMAPS* (2008).
14. P.G. Kim, K.N. Tu, and D.C. Abbott, *J. Appl. Phys.* 84, 770 (1998).
15. G. Ghosh, *J. Electron. Mater.* 28, 1238 (1999).
16. S.P. Peng, W.H. Wu, C.E. Ho, and Y.M. Huang, *J. Alloys Compd.* 493, 431 (2010).
17. W.H. Wu, H.L. Chung, C.N. Chen, and C.E. Ho, *J. Electron. Mater.* 38, 2563 (2009).
18. BGA Ball Shear, JESD22-B117, JEDEC Solid State Technology Association (2006).
19. C.E. Ho, R.Y. Tsai, Y.L. Lin, and C.R. Kao, *J. Electron. Mater.* 31, 584 (2002).
20. K. Zeng and K.N. Tu, *Mater. Sci. Eng.* R38, 55 (2002).
21. C.E. Ho, S.C. Yang, and C.R. Kao, *J. Mater. Sci.: Mater. Electron.* 18, 155 (2007).
22. Y.C. Lin and J.G. Duh, *Scripta Mater.* 54, 1161 (2006).
23. Y.C. Lin, T.Y. Shih, S.K. Tien, and J.G. Duh, *Scripta Mater.* 56, 49 (2007).
24. Y.C. Lin, K.J. Wang, and J.G. Duh, *J. Electron. Mater.* 39, 283 (2010).
25. Z.P. Xia, Y. Lin, and Z.Q. Li, *Mater. Charact.* 59, 1324 (2008).
26. J.W. Yoon and S.B. Jung, *J. Alloys Compd.* 396, 122 (2005).
27. S. Furuseth and H. Fjellvåg, *ACTA Chem. Scand. Ser. A* 39, 537 (1985).
28. H. Matsuki, H. Ibuka, and H. Saka, *Sci. Technol. Adv. Mater.* 3, 261 (2002).
29. S.W. Kim, J.W. Yoon, and S.B. Jung, *J. Electron. Mater.* 33, 1182 (2004).
30. Y.C. Sohn, J. Yu, S.K. Kang, D.Y. Shih, and T.Y. Lee, *J. Mater. Res.* 19, 2428 (2004).
31. S.J. Wang and C.Y. Liu, *Scripta Mater.* 49, 813 (2003).
32. C.E. Ho, Y.M. Chen, and C.R. Kao, *J. Electron. Mater.* 28, 1231 (1999).
33. G. Ghosh, *Acta Mater.* 48, 3719 (2000).
34. K.N. Tu, *Solder Joint Technology—Materials, Properties, and Reliability* (New York: Springer, 2007).
35. Y. Wang and K.N. Tu, *Appl. Phys. Lett.* 67, 1069 (1995).